

Article

Discovery of Novel PI3K δ Inhibitors Based on the p110 δ Crystal Structure

Wenqing Jia ^{1,†}, Shuyu Luo ^{2,†}, Wennan Zhao ¹, Weiren Xu ³, Yuxu Zhong ^{4,*} and Dexin Kong ^{1,*} 

¹ Tianjin Key Laboratory on Technologies Enabling Development of Clinical Therapeutics and Diagnostics, School of Pharmaceutical Sciences, Tianjin Medical University, Tianjin 300070, China

² School of Stomatology, Hospital of Stomatology, Tianjin Medical University, Tianjin 300070, China

³ Tianjin Institute of Pharmaceutical Research, Tianjin 300070, China

⁴ State Key Laboratory of Toxicology and Medical Countermeasures, Beijing Institute of Pharmacology and Toxicology, Beijing 100850, China

* Correspondence: yuxuzhong2008@aliyun.com (Y.Z.); kongdexin@tmu.edu.cn (D.K.)

† These authors contributed equally to this work.

Abstract: PI3K δ is a key mediator of B-cell receptor signaling and plays an important role in the pathogenesis of certain hematological malignancies, such as chronic lymphocytic leukemia. Idelalisib, which targets PI3K δ specifically, is the first approved PI3K inhibitor for cancer therapy. Recently, we carried out virtual screening, cell-based assays, adaption kinase assays, and molecular dynamic analysis to discover novel PI3K δ inhibitors and identified NSC348884 as a lead PI3K δ inhibitor. NSC348884 had an excellent docking score, potent PI3K δ -inhibitory activity, antitumor effects on various cancer cell lines, and a favorable binding mode with the active site of PI3K δ . Moreover, through the structural modification of NSC348884, we further discovered comp#1, which forms H-bonds with both Val828 and Lys779 in the ATP binding pocket of PI3K δ , with a more favorable conformation binding to PI3K δ . In addition, we found that N¹, N¹, N²-trimethyl-N²-((6-methyl-1H-benzo[d]imidazol-2-yl)methyl) ethane-1,2-diamine might be a potential scaffold structure. Thus, the result of this study provides a far more efficient approach for discovering novel inhibitors targeting PI3K δ .

Keywords: PI3K δ ; inhibitor; virtual screening; lead scaffold; cancer



Citation: Jia, W.; Luo, S.; Zhao, W.; Xu, W.; Zhong, Y.; Kong, D. Discovery of Novel PI3K δ Inhibitors Based on the p110 δ Crystal Structure. *Molecules* **2022**, *27*, 6211. <https://doi.org/10.3390/molecules27196211>

Academic Editor: Marilisa Leone

Received: 13 August 2022

Accepted: 14 September 2022

Published: 21 September 2022

Publisher's Note: MDPI stays neutral with regard to jurisdictional claims in published maps and institutional affiliations.



Copyright: © 2022 by the authors. Licensee MDPI, Basel, Switzerland. This article is an open access article distributed under the terms and conditions of the Creative Commons Attribution (CC BY) license (<https://creativecommons.org/licenses/by/4.0/>).

1. Introduction

Phosphoinositide 3-kinases (PI3Ks) are a conserved family of kinases that phosphorylate phosphatidylinositol 4,5-trisphosphate (PIP₂) to phosphatidylinositol 3,4,5-trisphosphate (PIP₃), which acts as a second messenger to activate downstream signaling molecules. This phosphorylation process can be reversed by PTEN [1]. According to sequence homology, substrate selectivity, and differences in regulatory subunits, PI3Ks are divided into three classes. Among them, class I PI3Ks are further divided into IA (PI3K α , β , and δ) and IB (PI3K γ). PI3K α and PI3K β are commonly expressed in all cells, while PI3K δ and PI3K γ are mainly expressed in hematopoietic cells and are closely related to immune system diseases [2]. Class II PI3Ks consist of three members: PI3KC2 α , which is involved in endocytosis, vesicle trafficking, and mitosis; PI3KC2 β , which acts in cell migration; and PI3KC2 γ , known to activate Akt2 and liver glycogen storage [3]. The sole member of class III is named Vps34, whose functions are related to endocytosis, vesicular trafficking, and autophagy [4]. Among the three classes of PI3Ks, class I has been most widely studied and is therefore usually referred to as PI3K.

PI3K δ , which consists of a catalytic subunit p110 δ and a regulatory subunit p85, is a key mediator of B-cell receptor signaling and plays an important role in the pathogenesis of certain hematological malignancies, such as chronic lymphocytic leukemia (CLL) [5]. The proliferation of various hematologic tumor cells can be blocked by PI3K δ inhibitors, and normal immune cells can survive in this process. Recent reports have demonstrated

that the PI3K δ isoform is associated with myeloid-cell-mediated immunosuppression in solid tumors [6], including head and neck squamous cell carcinoma (HNSCC) [7].

ZSTK474 is a pan class I PI3K inhibitor that shows the most potent inhibition against the PI3K δ isoform [8,9]. PI3K δ inhibitors include propeller-shaped and flat inhibitors. ZSTK474 is a flat inhibitor and mainly occupies the hinge region and affinity pocket of the ATP binding pocket of the catalytic subunit (p110 δ) of PI3K δ in a competitive way [10]. ATP can form hydrogen bonds with Val828 in the hinge region. The ATP-competitive PI3K inhibitors identified to date accept an H-bond from this valine residue. For ZSTK474, the oxygen of one of the morpholino groups acts as the hinge Val828 hydrogen bond acceptor. The benzimidazole group extends into the “affinity” pocket, where its nitrogen acts as a hydrogen bond acceptor for the primary amine of Lys779. Compared with the binding of ATP, ZSTK474 forms hydrogen bonds to the binding pocket, similar to those made by ATP. After exhibiting remarkable antitumor effect in preclinical studies, ZSTK474 has entered phase I/II clinical trials to evaluate its safety and therapeutic effect on patients with advanced solid malignancies (NCT01280487 and NCT01682473). However, acquired resistance after long-term treatment with ZSTK474 has been observed [11,12]. The crystal structure of the ZSTK474-PI3K δ active site (2WXL) has been elucidated via X-ray analysis [13], which provides the basis for the discovery of novel PI3K δ inhibitors.

Idelalisib is the only PI3K δ -specific inhibitor approved by the FDA and has shown solid antitumor efficacy clinically but was found to have various immune-mediated side effects, such as hepatotoxicity, pneumonitis, infection, and intestinal perforation [14,15]. To circumvent these problems, new PI3K δ inhibitors are required. Virtual screening followed by experimental validation has been demonstrated to be a highly efficient approach for discovering molecular-targeted lead compounds. By utilizing such an approach, we found potential PI3K δ inhibitors from the compound database established by our laboratory. In this work, we report the discovery of new PI3K δ small-molecule inhibitors through virtual database screening in combination with an MTT assay, adaption kinase assay, and molecular dynamics simulation [16] (Figure 1).

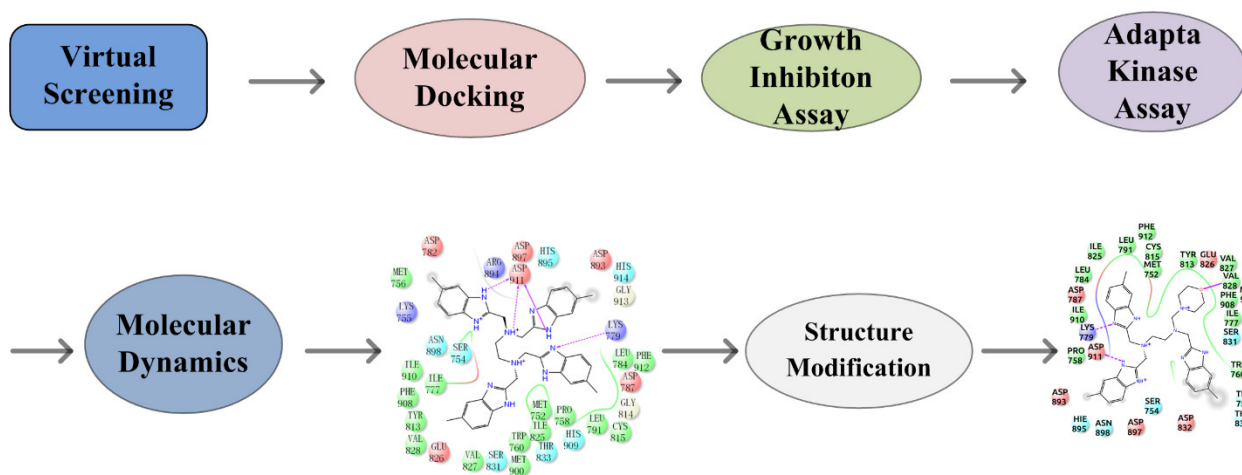


Figure 1. Flow chart of the discovery of the novel PI3K δ inhibitor.

2. Results and Discussion

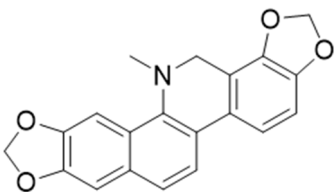
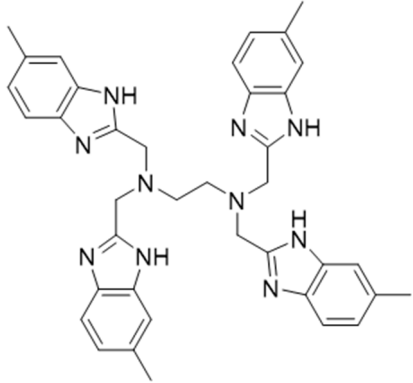
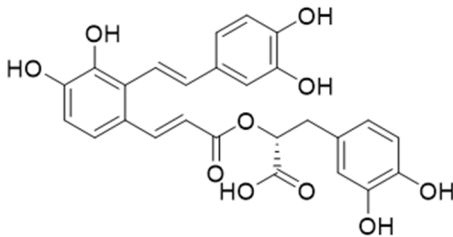
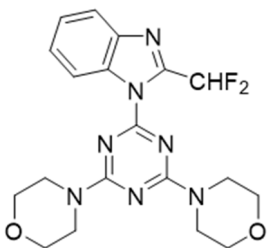
2.1. Virtual Screening of Potential PI3K δ Inhibitors

In this study, we used ZSTK474 as the positive drug to select compounds. Based on the results of HTVS and SP docking and by comparing docking scores and binding modes, seven commercially available compounds (Table 1) were selected from the database. The docking scores of all seven of these compounds are lower than that of ZSTK474.

Table 1. The structures and docking results of molecules.

Name	Structure	Docking Score (kcal/mol)
Rutin		−11.14
Pyridostatin		−10.69
Icariin		−10.35
Mulberroside A		−10.12

Table 1. Cont.

Name	Structure	Docking Score (kcal/mol)
Sanguinarine		−10.10
NSC348884		−9.69
Salvianolic acid A		−9.61
ZSTK474		−9.49

2.2. Antiproliferative Effect of the Screened Compounds

As the above seven compounds were screened as potential PI3K δ inhibitors, we tried to determine their antiproliferative activities on cancer cells possessing high PI3K δ expression. We searched the Cancer Cell Line Encyclopedia database (CCLE) for the PIK3CD gene expression levels in established cell lines and cross-compared them with the cell lines available in our lab. As shown in Figure 2, the PIK3CD gene expression levels in human chronic myelogenous leukemia K562 and human breast ductal carcinoma BT549 cells were relatively higher than in other cells. We then treated K562 and BT549 cells with the above seven compounds at 10 μ M for 48 h and determined the antiproliferative activity using the MTT assay. We found that three compounds (NSC348884, sanguinarine, and salvianolic acid A) inhibited the proliferation of K562 cells, with the viable cells reduced to 8.5%, 5.7%, and 17.3%, respectively, compared to the group without treatment. NSC348884 and sanguinarine exhibited similar antiproliferative effects in BT549 cells (14.7% and 18.4%, respectively), while salvianolic acid A only showed the minimum inhibition against BT549 cells (86.1% viable cells) (Figure 3).

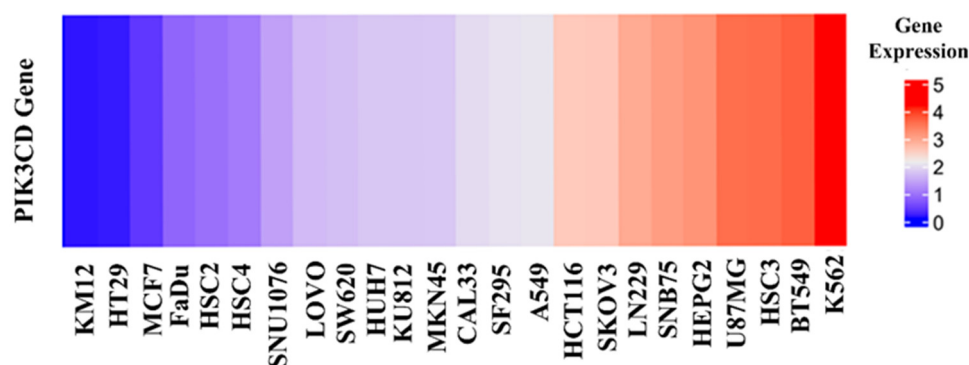


Figure 2. Gene expression levels in various cancer cell lines.

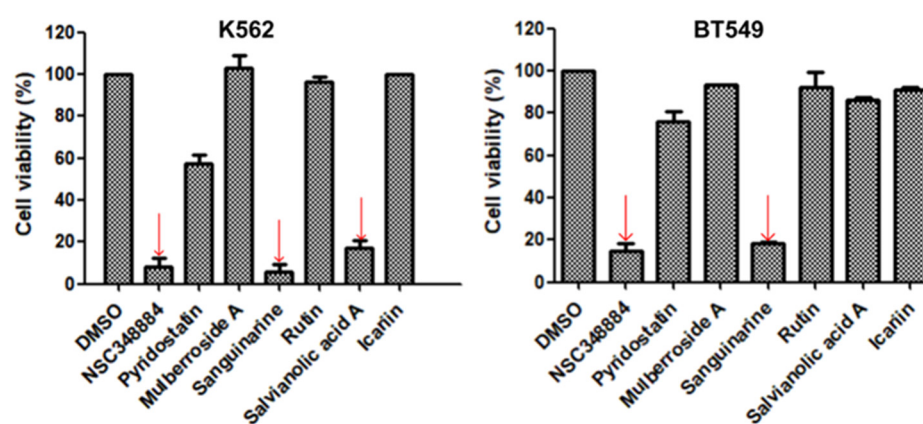


Figure 3. Effect of the selected compounds on cell viability of K562 and BT549 cells. The cells were treated with the seven compounds individually at 10 μ M for 48 h, and the cell viability was analyzed via the MTT assay. Data are presented as the mean \pm SD ($n = 3$).

2.3. PI3K δ -Kinase-Inhibitory Activities of the Selected Compounds

We then used the adaption kinase assay to determine the inhibition of the three compounds—NSC348884, sanguinarine, and salvianolic acid A—on the kinase activity of the recombinant PI3K δ . After treatment with 10 μ M of NSC348884 and sanguinarine, the activity of PI3K δ was reduced to 30.15% and 79.27%, respectively. Salvianolic acid A at 10 μ M, however, had no significant inhibitory effect on the kinase activity (Figure 4A). The IC_{50} value of NSC348884, the most potent inhibitor of the three compounds, was calculated to be 7.32 μ M, as shown in Figure 4B.

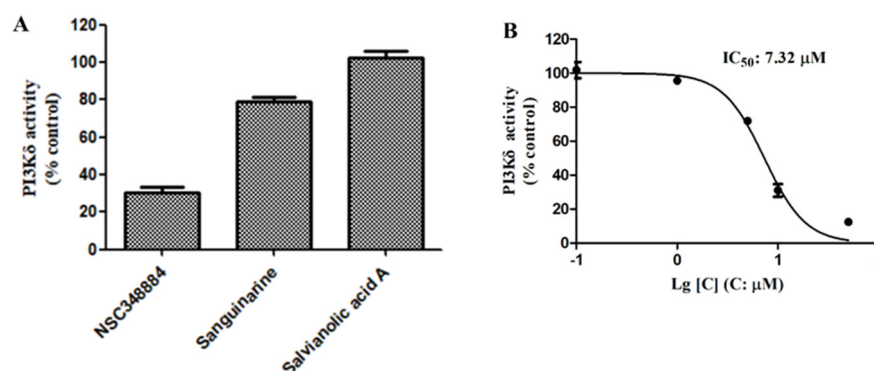


Figure 4. (A) Activities of 10 μ M of NSC348884, sanguinarine, and salvianolic acid A on PI3K δ . (B) NSC348884 inhibited PI3K δ in a concentration-dependent manner with an IC_{50} of 7.32 μ M. Data are presented as the mean \pm SD ($n = 3$).

2.4. The Mode of NSC348884 Binding to PI3K δ

Binding mode studies are of great significance for the discovery of more potent inhibitors based on the mechanism of the known inhibitors and PI3K δ . The morpholine oxygen atom of ZSTK474 was reported to form a key H-bond with the hinge region Val828, and the N3 of benzimidazole generated another H-bond with Lys779, consistent with our result (Figure 5A). Accordingly, we studied the mode of NSC348884 binding to PI3K δ . As shown in Figure 5B, NSC348884 bound to PI3K δ and formed multiple H-bonds with nearby residues, including Lys779 and Asp911. NSC348884 maintained the H-bond with the key amino acid Lys779, as found for ZSTK474. Asp911 formed H-bonds with two imidazole rings and amino groups of NSC348884. Compared with ZSTK474, NSC348884 had more H-bond interactions, which might be responsible for the lower docking score (ZSTK474-PI3K δ : -9.49 kcal/mol; NSC348884- δ : -9.69 kcal/mol). Figure 5C shows the superposition of ZSTK474 and NSC348884 in the binding pocket, and the binding mode of NSC348884 is indicated in Figure 5D. The benzimidazole group in NSC348884 basically overlaps with that of ZSTK474. This phenomenon also reasonably explains why both compounds formed the same H-bond with Lys779.

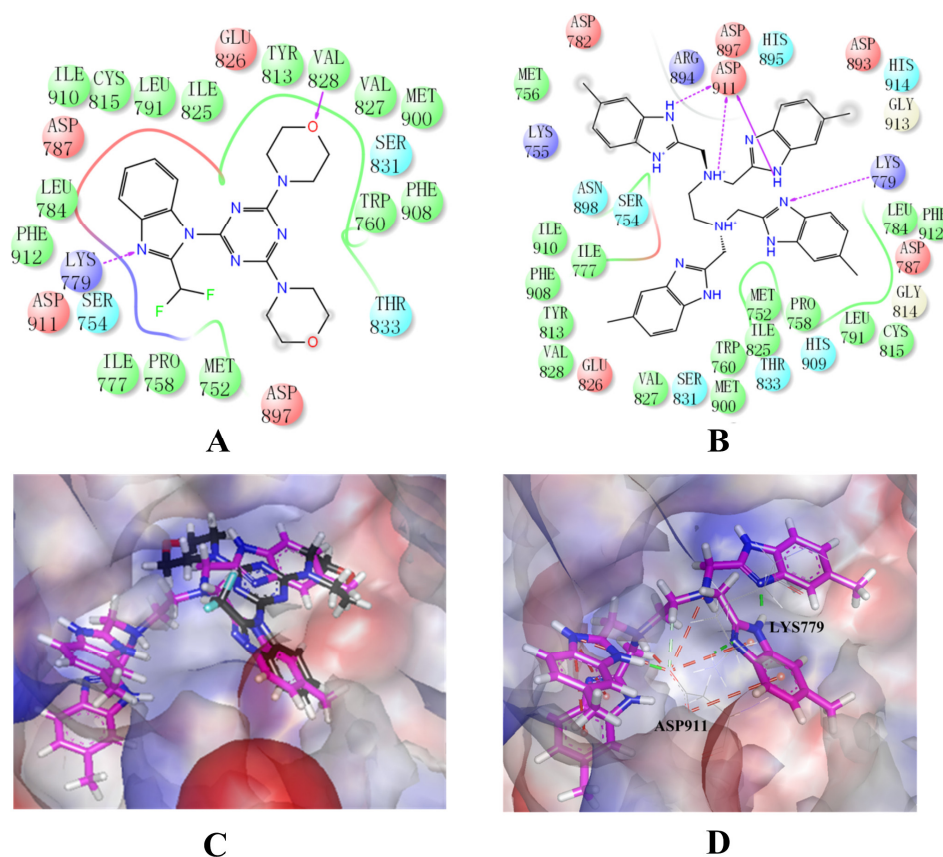


Figure 5. The predicted model of NSC348884 binding to the PI3K δ pocket. (A) A 2D diagram of ZSTK474-PI3K δ interactions in the PI3K δ pocket. (B) A 2D diagram of NSC348884-PI3K δ interactions in the PI3K δ pocket. (C) NSC348884 (purple)/ZSTK474 (black)-PI3K δ pocket. (D) NSC348884 (purple)-PI3K δ pocket.

2.5. Molecular Dynamics Simulations of NSC348884-PI3K δ

Molecular dynamics simulation is the investigation of the internal motions of a macromolecules as a function of time. The root mean square deviation (RMSD) is used to examine the stability and convergence of backbone C α atoms relative to the initial structure [17]. For PI3K δ without ligands, before 12 ns, the RMSD values experienced a rapid rise from 0 to 10.92 Å and then gradually tended to reach an equilibrium status (Figure 6A). In the

NSC348884-PI3K δ model, although the RMSD also increased initially, the value stabilized below 3.72 Å after 5 ns and then remained balanced (Figure 6A). In addition, the average RMSD value of NSC348884-PI3K δ was 2.68 Å, which was lower than that of the PI3K δ -without ligand system (7.76 Å) (Figure 6A). This shows that both systems reached the equilibrium condition after a short simulation, and NSC348884-PI3K δ was more stable. The root mean square fluctuation (RMSF) was used to calculate the average value of all atomic fluctuations [18]. Figure 6B shows the RMSF maps of PI3K δ -ligand complexes and PI3K δ during simulations. Overall, the fluctuation value for NSC348884-PI3K δ was lower than the PI3K δ -without ligand. The fluctuation values of Lys779 and Asp911 in NSC348884-PI3K δ were lower than the value in PI3K δ only, which suggests that the binding of NSC348884 to PI3K δ made the whole system more stable.

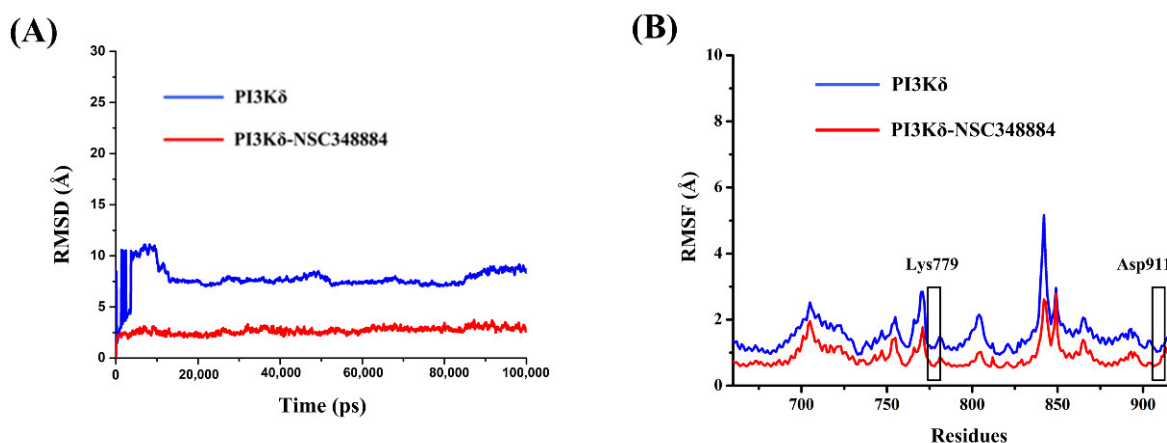


Figure 6. (A) The RMSD changes in NSC348884-PI3K δ complexes and PI3K δ during 100 ns simulations. (B) The RMSF changes in NSC348884-PI3K δ complexes and PI3K δ during 100 ns simulations. The boxes indicate the fluctuations of key residues (Lys779 and Asp911).

Figure 7 shows the interaction mode of NSC348884 and PI3K δ in the whole simulation process in the form of a histogram. A value above 1.0 indicates that there are multiple interactions between amino acid residues and ligands. H-bonds play important roles in the drug specificity, metabolic characteristics, absorption parameters, and blood–brain barrier permeability of drug candidates. For NSC348884-Asp911, the H-bond interaction fraction is 1.214 (>1.0), indicating that Asp911 binds with the ligand via multiple interactions of H-bonds, and the H-bonds are relatively stable (Figure 7 and Table 2). Lys779 can also form an H-bond with a ligand but mainly forms H-bonds with ligands indirectly through water molecules. In addition, during the simulation of 100 ns, Asp897 and Asn898 also form H-bonds with the ligand, and the H-bond occupancy are 13.5% and 9.2%, respectively. The hydrophobicity of Trp760 and Met900 also contributes to the stability of the whole system, and the occupancy of hydrophobic contacts is 50.3% and 38.6%, respectively.

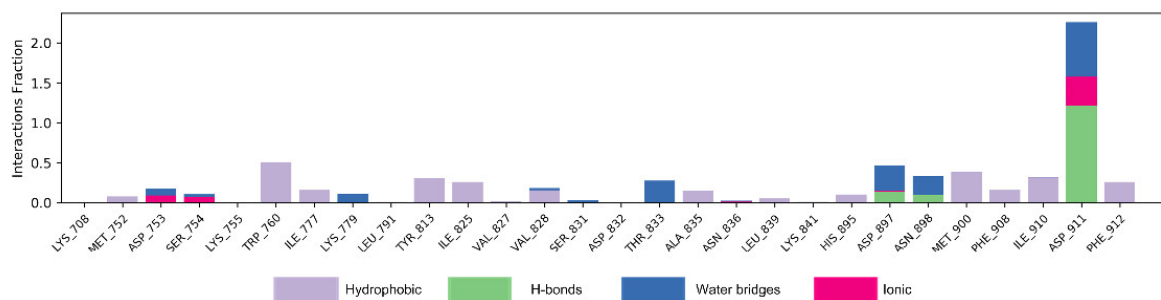


Figure 7. The bar charts of NSC348884-PI3K δ interactions. The legend for each color section is given.

Table 2. The occupancy of the protein–ligand interactions.

Ligand	Amino Acid	Occupancy of the Protein–Ligand Interactions (%)			
		H-Bonds	Hydrophobic Contacts	Ionic Interactions	Water Bridges
NSC348884	Trp760		50.3%		
	Ile777		15.9%		
	Tyr813		30.6%		
	Ile825		26.1%		
	Val828		15.4%		2.8%
	Ala835		14.9%		
	His895		10.2%		
	Met900		38.6%		
	Ile910		31.8%		0.1%
	Phe912		26%		
	Thr833				27.3%
	Lys779	0.3%			10.9%
	Asp897	13.5%		1.5%	31.7%
	Asn898	9.2%		0.1%	23.8%
	Asp911	>100% (1.214)		36.6%	68.1%

Note: For NSC348884-Asp911, the interaction fraction is 1.214 (>1.0), indicating Asp911 makes multiple interactions of H-bonds with the ligand.

2.6. Structural Modification of NSC348884

The above results suggest that NSC348884 might be a potential PI3K δ inhibitor. This finding provides a novel scaffold structure for the discovery of novel PI3K δ inhibitors. We further modified NSC348884 to improve its affinity. The designed structural modifications are shown in Figure 8. We analyzed and compared the structures of NSC348884 and ZSTK474, as well as the binding modes between the compounds and PI3K δ . To modify NSC348884, we tried the following approaches:

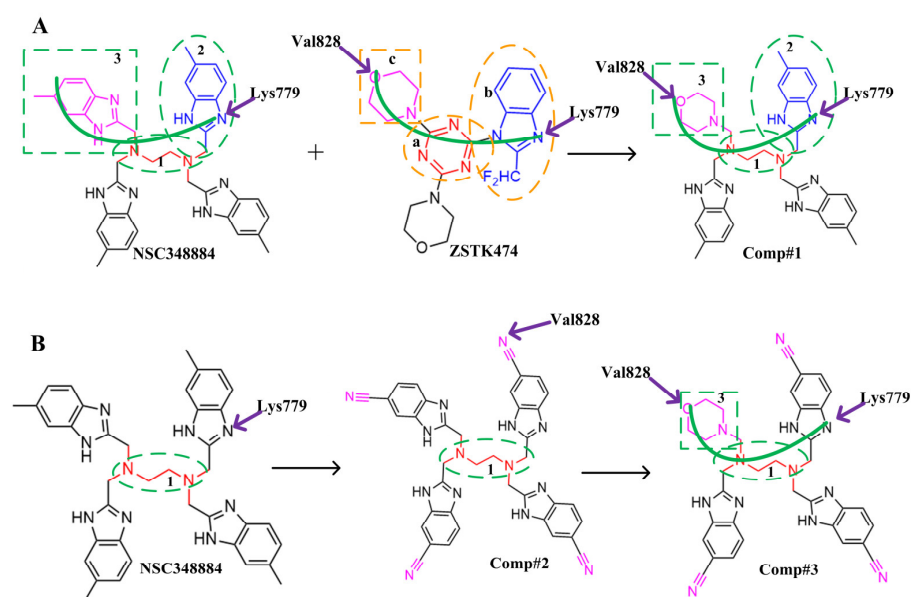


Figure 8. Schematic diagram of the structural modification of NSC348884. (A) Design of Comp#1 via structural modification of NSC348884; (B) design of Comp#2 and Comp#3 via structural modification of NSC348884. a: triazine; b: benzimidazole; c: morpholino; 1: tetramethylethane-1,2-diamine; 2: 6-methyl-benzimidazole.

(1) Both ZSTK474 and NSC348884 contain a benzimidazole group, and this group forms an H-bond with the key amino acid Lys779. As the main scaffold, the benzimidazole should be retained during modification (Figure 8A).

(2) ZSTK474 is a triazine derivative. The benzimidazole group extends into the “affinity” pocket, where its nitrogen acts as an H-bond acceptor for Lys779. The oxygen of the morpholino groups forms an H-bond with Val828 as the hinge H-bond acceptor. To improve the affinity of NSC348884 with the target, we introduced a group that can form an H-bond with Val828. We used tetramethylethane-1,2-diamine and 6-methyl-benzimidazole in NSC348884 as the scaffold structure. By analyzing the position of benzimidazole N3 and the oxygen atom on the morpholine ring in ZSTK474, we introduced a morpholine group to NSC348884 to obtain comp#1. A molecular docking study indicated that the docking score of comp#1 was -10.52 kcal/mol, lower than that of NSC348884 (-9.69 Kcal/mol). As expected, comp#1 formed H-bonds with Lys779 and Val828, and the H-bond with Asp911 remained (Figures 8A and 9A).

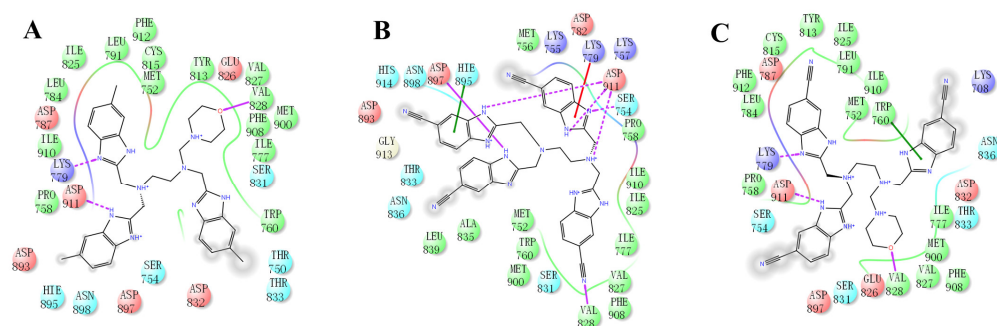


Figure 9. The predicted binding modes of comp#1 (A), comp#2 (B), and comp#3 (C) to the PI3K δ pocket. The 2D diagrams of comp#1/2/3-PI3K δ interactions in the PI3K δ pocket are indicated.

(3) The direct introduction of H-bond acceptors could form H-bonds with Val828 on 6-methyl-benzimidazole, as exhibited by Comp#2 (Figures 8B and 9B). The docking results showed the introduction of a nitrogen atom enabled comp#2 to form an H-bond with Val828, with a docking score lower than that of NSC348884. However, the H-bond at Lys779 disappeared. To achieve the dual purpose, we introduced a morpholine ring to comp#2 and obtained comp#3. The docking results showed that comp#3 could form H-bonds with Val828 and Lys779 (Figure 9C), with a docking score of -10.43 Kcal/mol, lower than that of comp#2.

(4) By comparing comp#1 with comp#3, we found that the mode of binding between comp#1 and PI3K δ was more similar to ZSTK474. In both compounds, Lys779 and Val828 could form H-bonds with nitrogen atoms in benzimidazole and oxygen atoms in the morpholine ring, respectively. The docking score of comp#1 was also lower than that of comp#3. Therefore, we chose comp#1 for further evaluation. The reason for the formation of H-bonds between comp#1 and Lys779/Val828 could also be explained by the superposition diagram of ZSTK474 and NSC348884/Comp#1 in the binding pocket. As shown in Figure 10, the benzimidazole basically overlapped, and the distance between the oxygen atoms on morpholine rings was close in the ZSTK474/NSC348884 superposition diagram (Figure 10). The degree of superposition determines the strength of H-bonds between compounds and key amino acids. Therefore, comp#1 has better affinity to PI3K δ . Detailed information on these three compounds is shown in Table 3.

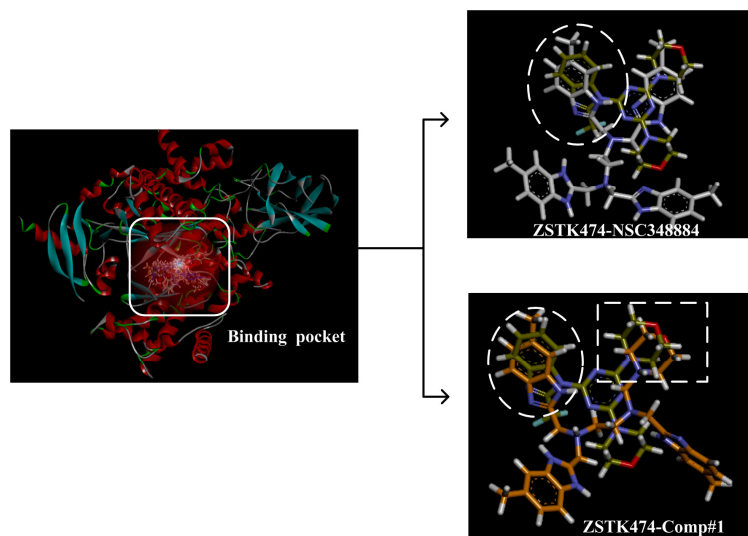


Figure 10. Superposition of ZSTK474/NSC348884 and ZSTK474/Comp#1. Grayish green: ZSTK474; white: NSC348884; orange: Comp#1.

Table 3. Structures and docking scores of the designed compounds.

Name	Structure	Docking Score (kcal/mol)
Comp#1		−10.52
Comp#2		−10.28
Comp#3		−10.43

3. Materials and Methods

3.1. Virtual Screening and Molecular Docking Study

The crystal structures of PI3K δ (ID: 2WXL with a resolution of 1.99 Å) were acquired from RCSB Protein Data Bank (PDB, www.rcsb.org, accessed on 6 September 2020). The ligand of PI3K δ , ZSTK474, was used as a positive control. The compound database containing 16,000 compounds was collated by our group, which mainly consists of the following compounds: FDA-approved drugs, drugs in the clinical research phase, and compounds with biological activity in preclinical studies. Both natural products and synthetic compounds are included in this database.

ZSTK474, a pan PI3K inhibitor with the most potent inhibitory activity towards the PI3K δ isoform, is under clinical trial evaluation for the therapy of advanced solid malignancies as an oral drug [12,19]. Since the crystal structure of ZSTK474-PI3K δ has been elucidated [20], ZSTK474 can be used as a reference ligand for the discovery of novel PI3K δ inhibitors. Molecular docking was applied using GLIDE software from the Schrödinger suite 2009 Software Package [21]. The proteins downloaded from PDB have missing residues. Protein repair uses the prime module of Schrodinger. Prime can be used to create homology models for use in simulations and to repair protein structures. Protein structures were prepared using the PrepWizard module. The optimization of the H-bond was performed using an exhaustive sampling option [22]. Under the Impref module, the OPLS_2005 force field was determined [23]. The active site was defined as an enclosing box at the centroid of the workspace ligand as selected in the receptor folder. The box size was determined by dock ligands with lengths ≤ 8.5 Å. Finally, under the application module, a docking grid was obtained.

The selected ligands from the compound library containing diverse chemical datasets were prepared in the Ligprep module. The possible ionization states were generated at a target pH of 7.0 ± 2.0 using Ionizer. Generate tautomers was selected by default. The tautomerizer generates up to 8 tautomers per ligand. At most, 32 stereoisomers per ligand were obtained with the option of “Retain specified chiralities (vary other chiral centers)”. [24]. The prepared molecules and PI3K δ protein were then subjected to high-throughput virtual screening (HTVS) [25]. Based on the HTVS results, the GLIDE SP (standard precision) module [26,27] was subsequently used to obtain new PI3K δ inhibitors. The interaction mechanisms between virtual hits and the receptor were evaluated at the molecular docking stage.

3.2. Cell Lines and Culture Conditions

The human chronic myelogenous leukemia K562 and human breast ductal carcinoma BT549 cell lines were purchased from Cell Resource Center, Peking Union Medical College (Beijing, China). Cells were cultured in Roswell Park Memorial Institute (RPMI) 1640 medium (HyClone, Cramlington, UK) (for K562) and Dulbecco's Modified Eagle Medium (DMEM, HyClone, Cramlington, UK) (for BT549), supplemented with 10% (*v/v*) fetal bovine serum (FBS, Biological Industries, Kibbutz Beit-Haemek, Israel), 100 U/mL of penicillin, and 10 $\mu\text{g/mL}$ of streptomycin at 37 °C in a humidified atmosphere containing 5% CO₂ [28].

3.3. Cell Proliferation Assay

As previously reported [29,30], K562 cells and BT549 cells were plated at 2×10^4 cells/well in 96-well plates. Cells were treated with or without compounds for 48 h. After that, 20 μL of MTT was added into 96-well plates and incubated for another 4 h at 37 °C. The culture medium was discarded, and 150 μL of DMSO was added into 96-well plates. The light absorbance was detected at a wavelength of 490 nm by using a microplate reader (iMark, Bio Rad, Hercules, CA, USA). Data were analyzed by using the GraphPad Prism 5 software.

3.4. Adapta Kinase Assay

To study the PI3K-inhibitory activity of compounds, the kinase activity of PI3K δ in the presence or absence of the compounds was measured using the adapta kinase assay [31]. The kinase reaction was manipulated in 10 μ L total volume of the reaction buffer containing diluted compounds, PI3K δ kinase, 2 mM DTT, 0.1 mM substrate, and 0.02 mM ATP, in a 384-well plate for 1 h at 28 ± 1 °C. Then, 5 μ L of buffer containing 30 mM EDTA, 6 nM antibody, and 12 nM tracer was added and incubated for 0.5 h at room temperature. The kinase activity remaining in each well was calculated according to the formula: kinase activity (% control) = (sample-minus enzyme control)/(plus enzyme control-minus enzyme control) \times 100. For the plus enzyme control, PI3K δ kinase was incubated with its substrate PIP2 and ATP in the absence of the test compound (sample), and for the minus enzyme control, the substrate PIP2 was incubated with ATP in the absence of the kinase and the test compound. Data were analyzed using the GraphPad Prism 5 software.

3.5. Molecular Dynamics Simulations Assay

The molecular dynamics (MD) simulations were performed by using Desmond v4.3 software to analyze the stability and conformational changes in ligands, proteins, and protein–ligand complexes through trajectory charts. Briefly, a successful MD process consists of the following six parts: preparing proteins, building a model system, relaxing the model system, running the simulation, viewing the trajectory, and analyzing the results.

We prepared protein using protein preparation wizard. To make the molecular dynamics more realistic, we added a solvent environment to mimic the real environment of humans. In this process, the water model and box shape were set to SPC and orthorhombic, respectively, in order to accommodate the water molecules in the system. We applied “Buffer” as the method to calculate the box size within the dimensions of 10 Å \times 10 Å \times 10 Å. Moreover, counter ions were added to electrically neutralize the system. Default salt (NaCl) with the approximately physiological concentration of 0.15 M was placed in the simulation box to set the ionic strength. Ultimately, the biological system consisting of proteins, ligands, explicit solvent (water molecules), counter ions, and salt was set up. Then, the minimization process was performed to relax the system into local energy minimization because the model system built using the system builder panel was not optimal. The system was minimized using a hybrid method of the steepest descent and the limited-memory Broyden–Fletcher–Goldfarb–Shanno algorithms. After minimization, this model system was submitted to MD simulation steps using the Desmond v4.3 package with the OPLS_2005 force field. The relaxation times in the coupled thermostat and barostat methods were fixed to 1 and 2 ps, respectively. We used a cut-off radius of 9.0 Å to handle short-range coulombic interactions and a smooth particle mesh Ewald (PME) method with a 10^{-9} tolerance to calculate the long-range coulombic interactions. The SHAKE algorithm was used to satisfy the hydrogen bond geometry constraints during simulation. The integration time model for ‘bonded’, ‘near’, and ‘far’ options were set to 2, 2, and 6 fs, respectively.

Before performing the real simulations, a series of short molecular simulation (the first seven stages) steps were performed to relax the model system. In detail, stage 1 mainly aimed to detect the system type and traits. In stage 2, the restraints were put on solute-heavy atoms with small time steps (100 ps, 10 K) under Brownian dynamics NVT condition. With restraints on solute-heavy atoms (12 ps, 10 K) under NVT and NPT conditions, the next two stages were performed. In the sixth stage after the solvate pocket had been skipped in stage 5, restraints were sequentially exerted on solute-heavy atoms for 12 ps (NPT). Next, the process of no restraints (24 ps) was performed with NPT in stage 7. Once the system was equilibrated after the above-mentioned steps, the 100 ns simulation task (stage 8) was conducted at 300 K and 1.01325 bar of pressure without any restrictions. After the simulation, the analysis was run using simulation interaction diagram and simulation event analysis panels [21].

4. Conclusions

While dozens of PI3K inhibitors, including PI3K δ inhibitors, are in clinical evaluation, only five PI3K inhibitors have been approved. As the first approved PI3K inhibitor, idelalisib was approved by the FDA in 2014 for the treatment of recurrent CLL in combination with rituximab, or as a single drug to cure recurrent follicular B cell non-Hodgkin's lymphoma (FL) and recurrent small lymphocytic lymphoma (SLL). Notably, idelalisib is the only approved PI3K δ -specific inhibitor. The delayed progress in the development of other PI3K δ inhibitors is due to failure to achieve the desired efficacy, probably because of limited bioavailability, unpredictable toxicity, or acquired resistance. Given these impediments, there remains an urgent need to develop novel PI3K δ inhibitors.

In our study, we aimed to find more effective PI3K δ inhibitors by using virtual screening, based on the interaction mechanism existing between PI3K δ and ZSTK474. Of the seven candidate compounds tested, NSC348884, sanguinarine, and salvianolic acid A showed remarkable inhibitory effects on the growth of tumor cells. The adaption kinase assay was performed to verify the direct target of the compounds. The results demonstrate that NSC348884 is a PI3K δ inhibitor. Then, SP and MD analyses were used to evaluate the binding stability of NSC348884-PI3K δ . The docking score of PI3K δ -NSC348884 was lower than that of PI3K δ -ZSTK474, and the compound formed H-bonds with Lys779 in the binding pocket.

Through analyses of the structure, molecular docking, and molecular dynamics of NSC348884/ZSTK474-PI3K δ , we found that NSC348884-PI3K δ binding is stable, and this binding excludes H-bond forming with Val828. Therefore, we hypothesized that the structure could be modified to form H-bonds with two key amino acids by introducing a morpholine ring into NSC348884. The result showed that benzimidazole in comp#1/ZSTK474 basically overlaps, and the distance between oxygen atoms on the two morpholine rings is also very close. H-bonds in comp#1 and ZSTK474 with Lys779 and Val828 formed on the same nitrogen atom and oxygen atom, and the docking score of comp#1 was lower than that of ZSTK474, suggesting that comp#1 might be a more effective PI3K δ inhibitor.

In summary, our study demonstrated that NSC348884 is a novel PI3K δ inhibitor, and the structure modification of NSC348884 generates comp#1, which was expected to have higher binding affinity. The PI3K δ -inhibitory activity as well as antitumor effects will be determined in the future. This work provides a rapid approach to find novel PI3K δ inhibitors, and N¹, N¹, N²-trimethyl-N²-((6-methyl-1H-benzo[d]imidazol-2-yl) methyl) ethane-1,2-diamine might be a potential scaffold structure for PI3K δ inhibitor development.

Author Contributions: Methodology, software, and validation, W.J., S.L. and W.Z.; software and validation, W.X.; writing—original draft preparation, W.J. and D.K.; writing—review and editing, Y.Z. and D.K. All authors have read and agreed to the published version of the manuscript.

Funding: This research was funded by the National Natural Science Foundation of China, grant number 82073890 and 82061148017.

Institutional Review Board Statement: Not applicable.

Informed Consent Statement: Not applicable.

Data Availability Statement: The data presented in this study are available on request from the corresponding authors.

Conflicts of Interest: The authors declare that they have no known competing financial interest or personal relationships that could have appeared to influence the work reported in this paper.

References

1. Gim, H.J.; Choi, Y.S.; Li, H.; Kim, Y.J.; Ryu, J.H.; Jeon, R. Identification of a Novel PPAR-gamma Agonist through a Scaffold Tuning Approach. *Int. J. Mol. Sci.* **2018**, *19*, 3032. [[CrossRef](#)]
2. Zhao, W.; Qiu, Y.; Kong, D. Class I phosphatidylinositol 3-kinase inhibitors for cancer therapy. *Acta Pharm. Sin. B* **2017**, *7*, 27–37. [[CrossRef](#)]

3. Gulluni, F.; De Santis, M.C.; Margaria, J.P.; Martini, M.; Hirsch, E. Class II PI3K Functions in Cell Biology and Disease. *Trends Cell Biol.* **2019**, *29*, 339–359. [[CrossRef](#)]
4. Murray, J.T.; Panaretou, C.; Stenmark, H.; Miaczynska, M.; Backer, J.M. Role of Rab5 in the recruitment of hVps34/p150 to the early endosome. *Traffic* **2002**, *3*, 416–427. [[CrossRef](#)]
5. Randis, T.M.; Puri, K.D.; Zhou, H.; Diacovo, T.G. Role of PI3Kdelta and PI3Kgamma in inflammatory arthritis and tissue localization of neutrophils. *Eur. J. Immunol.* **2008**, *38*, 1215–1224. [[CrossRef](#)]
6. Ali, K.; Soond, D.R.; Pineiro, R.; Hagemann, T.; Pearce, W.; Lim, E.L.; Bouabe, H.; Scudamore, C.L.; Hancox, T.; Maecker, H.; et al. Inactivation of PI(3)K p110delta breaks regulatory T-cell-mediated immune tolerance to cancer. *Nature* **2014**, *510*, 407–411. [[CrossRef](#)]
7. Davis, R.J.; Moore, E.C.; Clavijo, P.E.; Friedman, J.; Cash, H.; Chen, Z.; Silvin, C.; Van Waes, C.; Allen, C. Anti-PD-L1 Efficacy Can Be Enhanced by Inhibition of Myeloid-Derived Suppressor Cells with a Selective Inhibitor of PI3Kdelta/gamma. *Cancer Res.* **2017**, *77*, 2607–2619. [[CrossRef](#)]
8. Lonetti, A.; Cappellini, A.; Bertaina, A.; Locatelli, F.; Pession, A.; Buontempo, F.; Evangelisti, C.; Evangelisti, C.; Orsini, E.; Zamboni, L.; et al. Improving nelarabine efficacy in T cell acute lymphoblastic leukemia by targeting aberrant PI3K/AKT/mTOR signaling pathway. *J. Hematol. Oncol.* **2016**, *9*, 114. [[CrossRef](#)]
9. Van Dort, M.E.; Jang, Y.; Bonham, C.A.; Heist, K.; Palagama, D.S.W.; McDonald, L.; Zhang, E.Z.; Chenevert, T.L.; Luker, G.D.; Ross, B.D. Structural effects of morpholine replacement in ZSTK474 on Class I PI3K isoform inhibition: Development of novel MEK/PI3K bifunctional inhibitors. *Eur. J. Med. Chem.* **2022**, *229*, 113996. [[CrossRef](#)] [[PubMed](#)]
10. Kong, D.; Yamori, T. ZSTK474 is an ATP-competitive inhibitor of class I phosphatidylinositol 3 kinase isoforms. *Cancer Sci.* **2007**, *98*, 1638–1642. [[CrossRef](#)]
11. Wang, Y.; Liu, J.; Qiu, Y.; Jin, M.; Chen, X.; Fan, G.; Wang, R.; Kong, D. ZSTK474, a specific class I phosphatidylinositol 3-kinase inhibitor, induces G1 arrest and autophagy in human breast cancer MCF-7 cells. *Oncotarget* **2016**, *7*, 19897–19909. [[CrossRef](#)]
12. Kong, D.; Okamura, M.; Yoshimi, H.; Yamori, T. Antiangiogenic effect of ZSTK474, a novel phosphatidylinositol 3-kinase inhibitor. *Eur. J. Cancer* **2009**, *45*, 857–865. [[CrossRef](#)]
13. Yaguchi, S.-I.; Fukui, Y.; Koshimizu, I.; Yoshimi, H.; Matsuno, T.; Gouda, H.; Hirono, S.; Yamazaki, K.; Yamori, T. Antitumor Activity of ZSTK474, a New Phosphatidylinositol 3-Kinase Inhibitor. *J. Natl. Cancer Inst.* **2006**, *98*, 545–556. [[CrossRef](#)]
14. Lampson, B.L.; Kasar, S.N.; Matos, T.R.; Morgan, E.A.; Rassenti, L.; Davids, M.S.; Fisher, D.C.; Freedman, A.S.; Jacobson, C.A.; Armand, P.; et al. Idelalisib given front-line for treatment of chronic lymphocytic leukemia causes frequent immune-mediated hepatotoxicity. *Blood* **2016**, *128*, 195–203. [[CrossRef](#)]
15. Barr, P.M.; Saylor, G.B.; Spurgeon, S.E.; Cheson, B.D.; Greenwald, D.R.; O'Brien, S.M.; Liem, A.K.; McLntyre, R.E.; Joshi, A.; Abella-Dominicis, E.; et al. Phase 2 study of idelalisib and entospletinib: Pneumonitis limits combination therapy in relapsed refractory CLL and NHL. *Blood* **2016**, *127*, 2411–2415. [[CrossRef](#)] [[PubMed](#)]
16. Khan, M.A.; Jain, V.K.; Rizwanullah, M.; Ahmad, J.; Jain, K. PI3K/AKT/mTOR pathway inhibitors in triple-negative breast cancer: A review on drug discovery and future challenges. *Drug Discov. Today* **2019**, *24*, 2181–2191. [[CrossRef](#)]
17. Harada, R.; Shigeta, Y. Temperature-Shuffled Structural Dissimilarity Sampling Based on a Root-Mean-Square Deviation. *J. Chem. Inf. Model* **2018**, *58*, 1397–1405. [[CrossRef](#)]
18. Davies, A.; Levenson, M.S. Estimating the root mean square of a wave front and its uncertainty. *Appl. Opt.* **2001**, *40*, 6203–6209. [[CrossRef](#)]
19. Miller, M.S.; Mountford, S.J.; Pinson, J.A.; Zheng, Z.; Kunzli, M.; Patel, V.; Hogg, S.J.; Shortt, J.; Jennings, I.G.; Thompson, P.E. Development of single and mixed isoform selectivity PI3Kdelta inhibitors by targeting Asn836 of PI3Kdelta. *Bioorg. Med. Chem. Lett.* **2016**, *26*, 4790–4794. [[CrossRef](#)]
20. Berndt, A.; Miller, S.; Williams, O.; Le, D.D.; Houseman, B.T.; Pacold, J.I.; Gorrec, F.; Hon, W.C.; Liu, Y.; Rommel, C.; et al. The p110 delta structure: Mechanisms for selectivity and potency of new PI(3)K inhibitors. *Nat. Chem. Biol.* **2010**, *6*, 117–124. [[CrossRef](#)]
21. Jia, W.Q.; Jing, Z.; Liu, X.; Feng, X.Y.; Liu, Y.Y.; Wang, S.Q.; Xu, W.R.; Liu, J.W.; Cheng, X.C. Virtual identification of novel PPARalpha/gamma dual agonists by scaffold hopping of saroglitazar. *J. Biomol. Struct. Dyn.* **2018**, *36*, 3496–3512. [[CrossRef](#)]
22. Hasan, M.A.; Mazumder, M.H.; Chowdhury, A.S.; Datta, A.; Khan, M.A. Molecular-docking study of malaria drug target enzyme transketolase in Plasmodium falciparum 3D7 portends the novel approach to its treatment. *Source Code Biol. Med.* **2015**, *10*, 7. [[CrossRef](#)]
23. Liu, X.; Jing, Z.; Jia, W.Q.; Wang, S.Q.; Ma, Y.; Xu, W.R.; Liu, J.W.; Cheng, X.C. Identification of novel PPARalpha/gamma dual agonists by virtual screening, ADMET prediction and molecular dynamics simulations. *J. Biomol. Struct. Dyn.* **2018**, *36*, 2988–3002. [[CrossRef](#)]
24. Allen, B.K.; Mehta, S.; Ember, S.W.J.; Zhu, J.Y.; Schonbrunn, E.; Ayad, N.G.; Schurer, S.C. Identification of a Novel Class of BRD4 Inhibitors by Computational Screening and Binding Simulations. *ACS Omega* **2017**, *2*, 4760–4771. [[CrossRef](#)]
25. Damm-Ganamet, K.L.; Bembek, S.D.; Venable, J.W.; Castro, G.G.; Mangelschots, L.; Peeters, D.C.G.; McAllister, H.M.; Edwards, J.P.; Disepio, D.; Mirzadegan, T. A Prospective Virtual Screening Study: Enriching Hit Rates and Designing Focus Libraries to Find Inhibitors of PI3Kdelta and PI3Kgamma. *J. Med. Chem.* **2016**, *59*, 4302–4313. [[CrossRef](#)] [[PubMed](#)]
26. Saxena, S.; Durgam, L.; Guruprasad, L. Multiple e-pharmacophore modelling pooled with high-throughput virtual screening, docking and molecular dynamics simulations to discover potential inhibitors of Plasmodium falciparum lactate dehydrogenase (PfLDH). *J. Biomol. Struct. Dyn.* **2019**, *37*, 1783–1799. [[CrossRef](#)]

27. Kim, S.; Noh, J.; Gu, G.H.; Aspuru-Guzik, A.; Jung, Y. Generative Adversarial Networks for Crystal Structure Prediction. *ACS Cent. Sci.* **2020**, *6*, 1412–1420. [[CrossRef](#)]
28. Zhou, Q.; Chen, Y.; Chen, X.; Zhao, W.; Zhong, Y.; Wang, R.; Jin, M.; Qiu, Y.; Kong, D. In Vitro Antileukemia Activity of ZSTK474 on K562 and Multidrug Resistant K562/A02 Cells. *Int. J. Biol. Sci.* **2016**, *8*, 631–638. [[CrossRef](#)]
29. Peng, X.; Wang, Z.; Liu, Y.; Peng, X.; Liu, Y.; Zhu, S.; Zhang, Z.; Qiu, Y.; Jin, M.; Wang, R.; et al. Oxyfadichalcone C inhibits melanoma A375 cell proliferation and metastasis via suppressing PI3K/Akt and MAPK/ERK pathways. *Life Sci.* **2018**, *206*, 35–44. [[CrossRef](#)]
30. Zhang, S.; Peng, X.; Li, X.; Liu, H.; Zhao, B.; Elkabets, M.; Liu, Y.; Wang, W.; Wang, R.; Zhong, Y.; et al. BKM120 sensitizes glioblastoma to the PARP inhibitor rucaparib by suppressing homologous recombination repair. *Cell Death Dis.* **2021**, *12*, 546. [[CrossRef](#)]
31. Kong, D.; Dan, S.; Yamazaki, K.; Yamori, T. Inhibition profiles of phosphatidylinositol 3-kinase inhibitors against PI3K superfamily and human cancer cell line panel JFCR39. *Eur. J. Cancer* **2010**, *46*, 1111–1121. [[CrossRef](#)] [[PubMed](#)]